This is a preprint, the final version is subject to change, of the American Mineralogist (MSA)
Cite as Authors (Year) Title. American Mineralogist, in press.
DOI: https://doi.org/10.2138/am-2018-6203

Cesium Adsorption Isotherm on Swelling High-charged Micas from Aqueous Solutions: Effect of Temperature

Francisco J. Osuna,[a] Agustín Cota,[b] Esperanza Pavón,[c] M. Carolina Pazos[d] and María D. Alba.[a,1]

[a]Instituto Ciencia de Materiales de Sevilla (CSIC-Universidad de Sevilla). Avda. Américo Vespucio, 49.41092 Sevilla, Spain

[b]Laboratorio de Rayos-X. CITIUS. Avda. Reina Mercedes, 4. 41012 Sevilla, Spain

[c]Center for the Development of Nanoscience and Nanotechnology, CEDENNA, 9170124 Santiago, Chile

[d]Escuela de Ciencias Químicas, Universidad Pedagógica y Tecnológica de Colombia UPTC. Avda. Central del Norte, Vía Paipa, Tunja, 39-115 Boyacá, Colombia.

ABSTRACT

The potential use of a new family of synthetic swelling micas for cesium immobilization from aqueous solution was evaluate and the structural modifications after adsorption were analyzed. The results have revealed that they are good cesium adsorbents compared to natural clays and as the layer charge increases, the adsorption capacity and affinity increase. The cesium ions are adsorbed through a cation exchange mechanism but an inner sphere complex with the basal oxygens of the tetrahedral sheet is favored. These findings imply that is possible to design minerals with improved environmental applications.

[1] Corresponding author: *e-mail address:* alba@icmse.csic.es

Keywords: Cesium aqueous solution; synthetic mica; sorption isotherm; clay barrier; waste management

INTRODUCTION

Along with the rapid development of nuclear industries, the contamination of radionuclides in the environment is a point of attention worldwide (Steinhauser 2014). Cesium isotopes (^{137}Cs, $t_{1/2}$= 30 yr, and ^{135}Cs, $t_{1/2}= 2 \cdot 10^6$ yr) are one of the major constituents of the wastewater effluents from nuclear reprocessing units (Castrillejo et al. 2016) and due to their long half-lives and high solubility, they are the most hazardous nuclides in radioactive wastes. Given its chemical similarity to alkalis, Cs^+ is readily assimilated by terrestrial and aquatic organisms and can gradually accumulate in the biological food chain (Nakao et al. 2008; Poinssot et al. 1999). Cesium strongly and selectively interacts with the phyllosilicate fraction of soil, sediment, and suspended particles (Zachara et al. 2002) but the interaction of Cs^+ in a geological material is expected to be highly sensitive to the relative compositions of smectite/vermiculite and mica/illite (Fan et al. 2014).

The objective of any waste management is immobilization and isolation for the time necessary to lower its environmental activity and for this, a number of natural and artificial barriers are used. Numerous studies focused on using clays as a chemical barrier for retention and storage of radioactive materials have been reported, since they have a great capacity to adsorb and immobilize cations (Alba et al. 2001; Chorover et al. 2003; Rani and Sasidhar 2012; Takahashi et al. 1987; Villa-Alfageme et al. 2015). Clayey waste materials can retain radionuclides by sorption but also, under certain conditions, can produce a chemical reaction that generates new phases immobilizing the radioactive elements (Villa-Alfageme et al. 2015). Other features that make clays useful

for retention of radioactive waste are their low permeability and high swelling capacity for absorption of ions, which predetermine their use as sealing barriers in multi-barrier systems when an underground geological repository for spent nuclear fuel and high-level radioactive wastes is constructed (Linares 1993).

Up to now, bentonites (smectites ca. 90%) have been proposed as the best candidate for the barriers (Gregor 1969). The principal component of bentonites is a 2:1 layer phyllosilicate with lamellar charge between 0.2 and 0.8. It is well known that as the total charge increases the immobilization capacity of the clay increases (Weir 1965). Structural features that increase the reactivity of these 2:1 phyllosilicates are the presence of aluminum in the tetrahedral sheet and the total occupation of the octahedral sheet (Alba et al. 2001). In this sense, Alba et al. (Alba et al. 2006) have synthesized a swelling high-charged (4 eq/unit cell) mica, Na-Mica-4, which is able to rehydrate and swell and has a high cation exchange capacity, comparable to aluminum-rich zeolites. These micas have attracted considerable interest because of their exceptional adsorption capacity and selectivity of harmful cations (Alba et al. 2006; Franklin and Lee 1996; Garcia-Jimenez et al. 2016; Kodama et al. 2001; Paulus et al. 1992) and they constitute a promising material for Cs adsorption.

Hence, the aim of this study was: (i) to evaluate the potential use of synthetic swelling high-charged micas, Na-Mica-n (n=2 and 4, layer charge) for cesium immobilization at standard temperature and pressure conditions; (ii) to evaluate the effect of temperature on its adsorption capacity; and; (iii) to determine the adsorption mechanism (unspecific adsorption or specific adsorption) that occurs at different temperatures.

EXPERIMENTAL AND ANALYTICAL PROCEDURES

Chemicals and materials

Na-Mica-n (n = 2 and 4) was synthesized using the NaCl-melt method following a similar procedure to that described by Alba et al. (Alba et al. 2006). Their structural formulae are $Na_n[Si_{8-n}Al_n]Mg_6O_{20}F_4$, where *n* represents the charge per unit cell (n = 2 and 4). The starting materials employed were SiO_2, $Al(OH)_3$, MgF_2 and NaCl. Stoichiometric proportions of reactants were weighed and mixed in an agate mortar. The molar ratio between the reactants were $(8\text{-}n)SiO_2:(n/2)Al_2O_3:6MgF_2:(2n)NaCl$ (Alba et al. 2006). The heat treatments were carried out in closed Pt crucibles at 900 ºC over 15 h using a heating rate of 10 ºC·min^{-1}. The product was washed with distilled water and the solid was separated by filtration, dried at room temperature and then ground in an agate mortar.

Sorption equilibrium isotherm

Each batch test sample in the sorption experiments at room temperature (RT) was prepared in a 50 ml centrifuge tube, where 0.2 g of Na-Mica-4 was dispersed with 30 ml of a CsCl solution at different concentrations ranging between 0.01-25 meq/L, the maximum concentration allows for satisfying the theoretical cation exchange capacity of the Na-Mica-4. For comparison, an adsorption at an initial concentration of 1 meq/L was carried out in Na-Mica-2. The samples were equilibrated for 24 h in an end-over-end shaker at 50 r.p.m. The phases were separated by centrifugation at 10,000 rpm at 8 ºC for 25 min.

The sorption isotherm at 80 ºC was carried out in a hydrothermal bomb (Alba et al. 2006) where 0.2 g of Na-Mica-4 was mixed with 30 ml of a CsCl solution at different concentrations ranging between 1.5-25 meq/L and heated at 80 ºC for 24 h.

This is a preprint, the final version is subject to change, of the American Mineralogist (MSA)
Cite as Authors (Year) Title. American Mineralogist, in press.
DOI: https://doi.org/10.2138/am-2018-6203

99 The supernatants were preserved by adding HNO_3 and cool stored for subsequent Cs^+
100 analysis by inductively coupled plasma-mass spectrometry (ICP-MS). The difference
101 between Cs^+ concentrations measured before and after sorption reveals the amount of
102 adsorbed Cs^+ (C_s, meq/kg)

$$C_s = \left(C_i - C_{eq}\right) \cdot \frac{V}{m}$$

103 where the V (L) is the volume of the solution, m is the weight of the mica (kg), C_i
104 (meq/L) and C_{eq} (meq/L) are the concentration of the Cs^+ in initial and final solutions,
105 respectively.

106 The solids were dried at room temperature and characterized by X-ray diffraction
107 (XRD), SEM/EDX microscopy and MAS NMR spectroscopy.

108 The adsorption percentage and the distribution ratio (K_d, L/kg), were calculated as
109 follows:

$$\%\, Adsorption = \frac{C_i - C_{eq}}{C_i} \cdot 100$$

$$K_d = \frac{C_s}{C_{eq}}$$

110 The Freundlich adsorption isotherm is widely used for mathematical descriptions of
111 adsorption on a heterogeneous adsorbent surface (Veli and Alyuz 2007). This isotherm
112 gives an expression encompassing the surface heterogeneity and the exponential
113 distribution of active sites and their energy. It can be written as follows (Bhattacharyya
114 and Sen Gupta 2007):

$$C_s = K_F \cdot {C_{eq}}^{n_F}$$

115 K_F (L/kg) is the Freundlich constant, which is related to adsorption capacity, and n_F
116 (dimensionless) is the adsorption intensity. The Freundlich constant n_F is a measure of
117 the deviation from linearity adsorption (n_F=1). If n_F value is above 1, this implies that
118 the sorption process is chemical, but if n_F value is below 1, sorption is more likely a

119 physical process (Xi et al. 2014). The physical adsorption is that where the interaction
120 between cesium and the mica surface is through weak Van der Waals forces (i.e. cation-
121 exchanged reaction). However, if the cesium reacts with the mica, the adsorption
122 mechanism is through ionic bonding. In general, the chemical adsorption requires
123 higher temperatures than the physical one.
124
125 **Characterization Techniques**
126 The Cs^+ concentrations in the initial and final solutions were measured by ICP-
127 MS with an atomic emission spectrometer with inductively coupled source, Perkin
128 Elmer, Model DRC-e. Such equipment is settled in the Mass Spectrometry and
129 Chromatography Unit at the University of Cordoba, Spain.
130 X-ray diffraction (XRD) patterns were obtained at the CITIUS X-ray laboratory
131 (University of Seville, Spain) on a Bruker D8 Advance instrument equipped with a Cu
132 Kα radiation source operating at 40 kV and 40 mA. Diffractograms were obtained in the
133 2θ range of 3–70° with a step size of 0.015° and a step time of 0.1 s.
134 The morphology and elemental composition of the crystalline phases after the Cs
135 treatments were analyzed by scanning electron microscopy (SEM/EDX), using a JEOL
136 microscope (JSM 5400 Model) and working at 20 kV, which is installed in the
137 Microscopy Service of ICMS (CSIC-US). This equipment is connected to an energy
138 dispersive system X-ray (EDX) (Oxford Link ISIS) which allows chemical analysis of
139 samples using a detector of Si/Li with a Be window.
140 The analysis of short-range structural order was carried out by Solid State Magic
141 Angle Spinning-Nuclear Magnetic Resonance (MAS-NMR). Spectra were acquired
142 using single pulse programs on a Bruker DRX 400, equipped with a multinuclear probe.
143 Solid samples were packed in cylindrical zirconia rotors of 4 mm diameter and turned

144 under the magic angle at a frequency of 10 kHz. ^{29}Si spectra were acquired at a
145 frequency of 79.49 MHz, using pulse width values of 2.66 μs (π/2 = 7.98 μs), and a
146 delay time of 3 s. The chemical shift values were expressed in ppm, using
147 tetramethylsilane as an external reference.
148
149 **RESULTS**
150
151 The adsorbed amounts of Cs^+ and K_d values of the different scenarios have been
152 obtained from the ICP-MS analysis. Figure 1 shows a comparison of the adsorption
153 percentage and K_d values with temperature. The variation of adsorption percentage on
154 Na-Mica-4 versus the initial concentration (Fig 1a) shows a maximum adsorption of
155 80% at low concentrations that decreased with an increase of the initial concentration,
156 whereas the K_d values (Fig. 1b) decreased exponentially with increasing adsorbed
157 cesium.
158 At 80 °C, as at RT, the adsorption percentage and the K_d values decreased when
159 the initial solution concentration and adsorbed cesium increased. However, at 80 °C a
160 higher adsorption was observed at nonspecific sites but with higher affinity (low K_d
161 values, but higher than at RT) was observed (Galunin et al. 2010). This difference was
162 greater at low initial concentrations, at C_i=1.5 meq/L: K_d (L/kg)=311.1±13.60 (RT) vs
163 548.1± 4.66 (80 ºC) and % ads= 67.5±4.03 (RT) vs 78.5±0.14 (80 ºC). At the higher
164 initial concentration, the opposite occurred, at C_i=25.0 meq/L: K_d (L/kg)=91.4±3.95
165 (RT) vs 78.8±4.58 (80 ºC) and % ads= 37.9±1.83 (RT) vs 34.5± 1.31 (80 ºC).
166 The adsorption isotherm at both temperatures for Na-Mica-4 (Fig. 2) fitted to an
167 L-Type isotherm without a plateau being formed and, thus, the adsorption limits were
168 not reached (Limousin et al. 2007). In fact, the maximum value of adsorption was ca.

1587.7 meq/kg at RT and ca. 2307.6 meq/kg at 80 ºC, which is below the cation exchange capacity of 4694.8 meq/kg.

The SEM micro-scale images (Fig. 3) show that mica retained its laminar structure and, therefore, the adsorption did not cause delamination of the clay, a postulated mechanism by some authors (Vejsada et al. 2005), when Na^+ was exchanged by other alkaline cations of higher radius such as K^+. The swelling state of the layers was analyzed by XRD, and the XRD patterns of the samples after the adsorption (Fig. 4) showed *00l* reflections compatible with a basal spacing of 1.20-1.22 nm, which indicated that Cs^+ formed a hydration complex in the interlayer space (Alba et al. 2006). At both temperatures, a decrease of the basal space was observed with respect to Na-Mica-4 when the initial Cs^+ concentration increased. Even at 80 ºC, no XRD reflections due to formation of new crystalline phases were observed (Fig. 5).

In the case of samples after adsorption of cesium at 80 ºC, a study by ^{29}Si MAS NMR (Fig. 6) was carried out in order to detect if the temperature could favor the nucleation of new phases that could not be observed by XRD. The initial Na-Mica-4 spectrum showed a set of signals between -75 and -100 ppm due to Q^3(nAl) with n=0, 1, 2 and 3 environments typical of micas (Sanz and Serratosa 1984). After adsorption at 80 ºC, the same set of signals with a gradual shift towards lower frequencies was observed.

DISCUSSION

The moderate K_d values indicated adsorption predominantly in nonspecific sites (Galunin et al., 2010) but the observation that it exponentially decreases with increasing adsorbed cesium (Fig. 1b) could indicate that there are interlayer adsorption sites of different specificity (Sposito et al., 1999):

- Site I: High affinity sites: the interlayer cation could form inner-sphere complexes by partial incorporation into the pseudo-hexagonal holes of the tetrahedral sheet..

- Site II: Low-affinity sites: the interlayer cation could form outer-sphere complexes as a hydrated interlayer cation.

Figure 1b shows that at low concentrations of adsorbed cesium the adsorption in the high-affinity site is higher at 80 ºC than at RT (higher K_d values) because the temperature favors the interaction with basal oxygens and an inner-sphere complex being favored. However, the observed convergence of K_d values where high adsorbed cesium is indicated, inferred that the adsorption on site II occurred after all of site I was occupied.

In order to evaluate the adsorption capacity of the synthetic high-charged micas (Na-Mica-n) with conventional adsorbents and to analyze the effect of the layer charge, Table 1 summarizes the adsorption values obtained from the Na-Mica-n and from the natural clays (Galambos et al. 2009; García-Gutiérrez 2010; Oztop and Shahwan 2006; Saxena et al. 2003). First, it was noted that synthetic micas, Na-Mica-n, adsorbed more Cs^+ than some of the natural clays. This result is remarkable considering that the experimental conditions in the case of micas are unfavorable since the ratio adsorbent:solution (S/L, g/L) is much higher in the case of natural clay assays (Wu et al. 2009). When comparing the percentage of adsorption between both synthetic micas studied here, a major adsorption capacity was observed as the lamellar charge increased (Na-Mica-4 > Na-Mica-2). In all cases, the main adsorption mechanism was in nonspecific sites and, thus, the adsorption capacity was governed by the mineral cation exchange capacity (CEC).

This is a preprint, the final version is subject to change, of the American Mineralogist (MSA)
Cite as Authors (Year) Title. American Mineralogist, in press.
DOI: https://doi.org/10.2138/am-2018-6203

Comparing the K_d values of Na-Mica-n and those from the literature (Table 1) shows that the specificity of the adsorption sites on the Na-Mica-4 are higher than those of Na-Mica-2, which can be justified because the cation amount necessary to satisfy the charge is half of that required in Na-Mica-2. Thus, the cations in Na-Mica-2 has less interaction with basal oxygens, as demonstrated by the analysis of the *b*-parameter values of the unit cell (Pavon et al. 2014). In general, the K_d values of Na-Mica-4 were higher than natural clays and fluoro-phlogopite gel, even when the ratio of adsorbent:solution (g/l) was much lower. In some cases, the initial concentration was much higher in the case of Na-Mica-n, both being unfavorable conditions for the adsorption parameters (Wu et al. 2009).

The maximum value of adsorption at both temperatures (RT and 80˚C; Fig. 2) was below the cation exchange capacity of Na-Mica-4. This fact has been previously observed with alkali cations, specifically, Park et al. (Park et al., 2012a) observed that when Na-Mica-4 was subjected to a process of cation exchange with K^+ or Rb^+ only half of the Na^+ was replaced, hydronium ions were generated and they only partially balanced the layer charge. In fact, the EDX composition map (Fig; 3) showed that the distribution of cesium was similar to that of sodium indicating that the cesium replaced the sodium in the interlayer space, although not completely. This reinforces that the adsorption of cesium is by a cation exchange mechanism as previously reported, and in accordance with the low K_d values.

An in depth analysis of the isotherm data was performed using the Freundlich model (Table 2) and the experimental data fit to two lines with different slopes supporting the two aforementioned interpretation of adsorption sites (Vejsada et al., 2005):

-Site I: The K_F values were high at both temperatures; at 80 ºC being higher, which indicates that the site I was a site of high adsorption affinity. The n_F value at RT was close to one which denotes a uniformity of the surface, which drastically diminishes at 80 ºC. The diminishing of n_F with temperature indicates that the adsorption bonds become weak at high temperature, and thus the cesium adsorption on site I is exothermic (Xi et al., 2014).

- Site II: The K_F values are lower than those in site I at both temperatures; at 80 ºC being even lower, which indicates that the site II was a site of lower adsorption affinity and corresponds to adsorption in the outer sphere as an interlayer hydrated cation. The n_F value at both temperatures was ca. 0.65 which shows that the clay surface charge is heterogeneous.

In both sites, the n_F values were lower than the unit, which indicates that the adsorption is by a physical process, through a cation exchange mechanism in sites with variable cation affinity (Harter and Baker 1977). Freundlich type sorption implies that there are at least two distinct sorption sites for Cs^+ as on illite (Poinssot et al. 1999). The "frayed edge" site, site I, dominates Cs^+ uptake at low concentration and the Na^+ ions compete but only at concentrations of orders of magnitude higher than Cs^+. Such sites are common in illite but are not generally associated with other clay minerals (Bradbury and Baeyens 2000). The second class of site (Site II) is the "planar site" (basal siloxane surface) and it is associated with the fixed negative charge on the tetrahedral sheet.

If we compare these data with those of natural clays, (Table 3) the Na-Mica-4 exhibited higher values of the K_F constant. Therefore, the Na-Mica-4 have greater affinity for cesium adsorption (Turiel et al., 2003). Moreover, the adsorption surface of Na-Mica-4 is more homogeneous than that of natural clays.

This is a preprint, the final version is subject to change, of the American Mineralogist (MSA)
Cite as Authors (Year) Title. American Mineralogist, in press.
DOI: https://doi.org/10.2138/am-2018-6203

After adsorption at high concentration, the basal spacing of the layered structure diminishes due to the lower hydration energy of cesium (264 kJ/mol) versus sodium (519 kJ/mol), which favors the formation of inner complexes with the basal oxygen for Cs^+ (Anderson and Sposito 1991, 1992). The absence of new phases containing cesium documented by XRD (Fig. 5) and ^{29}Si MAS NMR (Fig. 6) agrees with the n_F values that indicate Cs^+ was bonded by weak electrostatic (Van der Waals) interactions.

However, the gradual shift of the set of ^{29}Si MAS NMR signals towards lower frequencies indicates a participation of the inner-sphere complex. Those complexes imply that cesium is partially located in the pseudo-hexagonal holes of the tetrahedral sheet, interacting with the basal oxygens, and, thus, modifying the angle of rotation of the tetrahedra (Limousin et al. 2007).

IMPLICATIONS

We have demonstrated that synthetic micas, Na-Mica-n, are better adsorbents of cesium from aqueous solution than natural clays. The adsorption capacity and affinity increases as the layer charge of micas increase. The cesium isotherm followed the Freundlich model and the fit parameters pointed to a physical adsorption by a cation exchange mechanism at both temperatures. At higher temperature (80˚C) an increase of the Cs-adsorption was observed in higher affinity sites without actually modifying the mica structure, because the adsorption is thorough cation exchange but with higher participation of the inner-sphere complex. These results show that minerals can be designed with improved environmental applications.

This is a preprint, the final version is subject to change, of the American Mineralogist (MSA)
Cite as Authors (Year) Title. American Mineralogist, in press.
DOI: https://doi.org/10.2138/am-2018-6203

ACKNOWLEDGEMENTS

We would like to thank the Junta de Andalucía (Spain) and FEDER (Proyecto de Excelencia de la Junta de Andalucía, project P12-FQM-567), to the Spanish State Program R+D +I oriented societal challenges and FEDER (Project MAT2015-63929-R) and ENRESA (contract nº 0079000237) for financial support. Dr. Pavón thanks her grant to Andalucía Talent Hub Program, co-funded by the EU in 7FP, Marie Skłodowska-Curie actions (nº 291780) and the Junta de Andalucía. F.J. Osuna thanks his grant to the training researcher program associated to the excellence project of Junta de Andalucía (P12-FQM-567).

REFERENCES CITED

Alba M.D., Becerro A.I., Castro M.A. and Perdigon A.C. (2001) Hydrothermal reactivity of Lu-saturated smectites: Part II. A short-range order study. Am. Miner. 86, 124-131.

Alba M.D., Castro M.A., Naranjo M. and Pavon E. (2006) Hydrothermal reactivity of Na-n-micas (n=2, 3, 4). Chem. Mat. 18, 2867-2872.

Anderson S.J. and Sposito G. (1991) Cesium-adsorption method for measuring accessible structural surface-charge. Soil Sci. Soc. Am. J. 55, 1569-1576.

Anderson S.J. and Sposito G. (1992) Proton surface-charge density in soils with structural and ph-dependent charge. Soil Sci. Soc. Am. J. 56, 1437-1443.

Bhattacharyya K.G. and Sen Gupta S. (2007) Adsorptive accumulation of Cd(II), Co(II), Cu(II), Pb(II), and Ni(II) from water on montmorillonite: Influence of acid activation. J. Colloid Interface Sci. 310, 411-424.

Bradbury M.H. and Baeyens B. (2000) A generalised sorption model for the concentration dependent uptake of caesium by argillaceous rocks. J. Contam. Hydrol. 42, 141-163.

Castrillejo M., Casacuberta N., Breier C.F., Pike S.M., Masque P. and Buesseler K.O. (2016) Reassessment of Sr-90, Cs-137, and Cs-134 in the Coast off Japan Derived from the Fukushima Dai-ichi Nuclear Accident. Environ. Sci. Technol. 50, 173-180.

Chorover J., Choi S.K., Amistadi M.K., Karthikeyan K.G., Crosson G. and Mueller K.T. (2003) Linking cesium and strontium uptake to kaolinite weathering in simulated tank waste leachate. Environ. Sci. Technol. 37, 2200-2208.

374 Fan Q.H., Tanaka M., Tanaka K., Sakaguchi A. and Takahashi Y. (2014) An EXAFS
375 study on the effects of natural organic matter and the expandability of clay
376 minerals on cesium adsorption and mobility. Geochim. Cosmochim. Acta 135,
377 49-65.
378 Franklin E.R. and Lee E. (1996) Synthesis and ion-exchange properties of Na-4-mica. J.
379 Mater. Chem. 6, 109-115.
380 Galambos M., Kufcakova J. and Rajec P. (2009) Adsorption of cesium on domestic
381 bentonites. J. Radioanal. Nucl. Chem. 281, 485-492.
382 Galunin E., Alba M.D., Santos M.J., Abrao T. and Vidal M. (2010) Lanthanide sorption
383 on smectitic clays in presence of cement leachates. Geochim. Cosmochim. Acta
384 74, 862-875.
385 García-Gutiérrez M.M., T.; Mingarro, M. (2010) Ensayos de sorción de 137Cs por la
386 muestra "rojo carbonero" para su empleo en la construcción de una barrera
387 reactiva permeable, CRI-9 (Huelva). CIEMAT, Madrid.
388 Garcia-Jimenez M.J., Cota A., Osuna F.J., Pavon E. and Alba M.D. (2016) Influence of
389 temperature and time on the Eu3+ reaction with synthetic Na-Mica-n (n=2 and
390 4). Chem. Eng. J. 284, 1174-1183.
391 Gregor M.C., B. (1969) Bentonite and its use. SAV, Bratislava.
392 Harter R.D. and Baker D.E. (1977) Applications and misapplications of Langmuir
393 equation to soil adsorption phenomena. Soil Sci. Soc. Am. J. 41, 1077-1080.
394 Kodama T., Harada Y., Ueda M., Shimizu K., Shuto K. and Komarneni S. (2001)
395 Selective exchange and fixation of strontium ions with ultrafine Na-4-mica.
396 Langmuir 17, 4881-4886.

Limousin G., Gaudet J.P., Charlet L., Szenknect S., Barthes V. and Krimissa M. (2007) Sorption isotherms: A review on physical bases, modeling and measurement. Appl. Geochem. 22, 249-275.

Linares J.H., F.; Cuadros, F.J. (1993) Comportamiento geoquímico de barreras arcillosas: Transformaciones hidrotermales en esmectitas alúmicas. Estudios Geol. 49, 127-136.

Nakao A., Thiry Y., Funakawa S. and Kosaki T. (2008) Characterization of the frayed edge site of micaceous minerals in soil clays influenced by different pedogenetic conditions in Japan and northern Thailand. Soil Sci. Plant Nutr. 54, 479-489.

Oztop B. and Shahwan T. (2006) Modification of a montmorillonite-illite clay using alkaline hydrothermal treatment and its application for the removal of aqueous Cs+ ions J. Colloid Interface Sci. 295, 303-309.

Park Y., Shin W.S. and Choi S.J. (2012) Removal of Co, Sr and Cs from aqueous solution using self-assembled monolayers on mesoporous supports. Korean J. Chem. Eng. 29, 1556-1566.

Paulus W.J., Komarneni S. and Roy R. (1992) Bulk synthesis and selective exchange of strontium ions in Na4Mg6Al4Si4O20F4 mica. Nature 357, 571-573.

Pavon E., Castro M.A., Cota A., Osuna F.J., Pazos M.C. and Alba M.D. (2014) Interaction of Hydrated Cations with Mica-n (n=2, 3 and 4) Surface. J. Phys. Chem. C 118, 2115-2121.

Poinssot C., Baeyens B. and Bradbury M.H. (1999) Experimental and modelling studies of caesium sorption on illite. Geochim. Cosmochim. Acta 63, 3217-3227.

Rani R.D. and Sasidhar P. (2012) Sorption of Cesium on Clay Colloids: Kinetic and Thermodynamic Studies. Aquat. Geochem. 18, 281-296.

Sanz J. and Serratosa J.M. (1984) Si-29 and Al-27 high-resolution mas-nmr spectra of phyllosilicates. J. Am. Chem. Soc. 106, 4790-4793.

Saxena A., Tomar R., Murali M.S. and Mathur J.N. (2003) Sorption of Am(III), U(VI) and Cs(I) on sodium potassium fluorophlogopite, an analogue of the fluorine mica mineral. J. Radioanal. Nucl. Chem. 258, 65-72.

Steinhauser G. (2014) Fukushima's Forgotten Radionuclides: A Review of the Understudied Radioactive Emissions. Environ. Sci. Technol. 48, 4649-4663.

Takahashi M., Muroi M., Inoue A., Aoki M., Takizawa M., Ishigure K. and Fujita N. (1987) Properties of bentonite clay as buffer material in high-level waste geological disposal .1. Chemical-species contained in bentonite. Nucl. Technol. 76, 221-228.

Vejsada J., Hradil D., Randa Z., Jelinek E. and Stulik K. (2005) Adsorption of cesium on Czech smectite-rich clays - A comparative study. Appl. Clay Sci. 30, 53-66.

Veli S. and Alyuz B. (2007) Adsorption of copper and zinc from aqueous solutions by using natural clay. J. Hazard. Mater. 149, 226-233.

Villa-Alfageme M., Hurtado S., El Mrabet S., Pazos M.C., Castro M.A. and Alba M.D. (2015) Uranium immobilization by FEBEX bentonite and steel barriers in hydrothermal conditions. Chem. Eng. J. 269, 279-287.

Weir A.H. (1965) Potassium retention in montmorillonite. Clay Miner. 6, 17-22.

Wu J.J., Li B., Liao J.L., Feng Y., Zhang D., Zhao J., Wen W., Yang Y.Y. and Liu N. (2009) Behavior and analysis of Cesium adsorption on montmorillonite mineral. J. Environ. Radioact. 100, 914-920.

Xi J.H., He M.C. and Zhang G.Z. (2014) Antimony adsorption on kaolinite in the presence of competitive anions. Environ. Earth Sci. 71, 2989-2997.

445 Zachara J.M., Smith S.C., Liu C.X., McKinley J.P., Serne R.J. and Gassman P.L. (2002)
446 Sorption of Cs+ to micaceous subsurface sediments from the Hanford site, USA.
447 Geochim. Cosmochim. Acta 66, 193-211.

448

This is a preprint, the final version is subject to change, of the American Mineralogist (MSA)
Cite as Authors (Year) Title. American Mineralogist, in press.
DOI: https://doi.org/10.2138/am-2018-6203

304

TABLE 1. Adsorption parameters for Cs^+ sorption on Na-Mica-n (n=2 and 4) and natural clays at RT.

	C_i meq/L	S/L[a] g/ml	K_d L/kg	% Ads.	Ref.
Na-Mica-4	10^{-2}	$7\cdot10^{-3}$	549.2	78.5	[b]
	1	$7\cdot10^{-3}$	367.5	71.0	[b]
Na-Mica-2	10^{-2}	$7\cdot10^{-3}$	396.5	68.1	[b]
Bentonite Rojo carbonero	$3\cdot10^{-6}$	$1\cdot10^{-1}$	497.0	--	[c]
Sediment St. Juan (Huelva)	$3\cdot10^{-6}$	$1\cdot10^{-1}$	664.0	--	[c]
Sepiolite	$3\cdot10^{-6}$	$1\cdot10^{-1}$	381.7	--	[c]
Fluorphlogopite	10^{-2}	$2\cdot10^{-2}$	80	--	[d]
gel	1	$2\cdot10^{-2}$	63	--	[d]
Clay MI	1	$1\cdot10^{-2}$	--	44.0	[e]
Clay MIS	1	$1\cdot10^{-2}$	--	65.0	[e]
Clay MID	1	$1\cdot10^{-2}$	--	89.0	[e]
Bentonite J45	1	$1\cdot10^{-2}$	785	72	[f]
Bentonite K45	1	$1\cdot10^{-2}$	478	72	[f]
Bentonite L45	1	$1\cdot10^{-2}$	296	36	[f]
Bentonite LA45	1	$1\cdot10^{-2}$	214	32	[f]

[a] the ratio adsorbent:solution
[b] this work; [c] (García-Gutiérrez 2010); [d] (Saxena et al. 2003); [e] (Oztop and Shahwan 2006); [f] (Galambos et al. 2009)

This is a preprint, the final version is subject to change, of the American Mineralogist (MSA)
Cite as Authors (Year) Title. American Mineralogist, in press.
DOI: https://doi.org/10.2138/am-2018-6203

305

306

TABLE 2. Parameters from Freundlich isotherm equation for the adsorption of Cs^+ on Na-Mica-4, at RT and 80 ºC.

T (ºC)	Site I			Site II		
	K_F L/kg	n_F	R^2	K_F L/kg	n_F	R^2
RT	288.14±1.09	0.90±0.02	0.996	235.70±1.04	0.63±0.03	0.992
80	336.59±1.02	0.57±0.03	0.995	219.72±1.15	0.65±0.05	0.989

307

308

309

TABLE 3. Parameters from Freundlich isotherm equations for the adsorption of Cs^+ on natural clays.

	K_F L/kg	n_F	Ref.
SAMMS	$2.18 \cdot 10^{-4}$	0.45	[a]
SAz-1	176.00	0.91	[b]
S-Tx-1	60.68	0.84	[b]
IMt-1	1.63	0.61	[b]
KGa-2	0.70	0.67	[b]
Mont-Ill-MI	2.95	0.52	[c]
Mont-Ill-MIS	12.00	0.62	[c]
Mont-Ill-MID	63.10	0.69	[c]

[a] (Park et al. 2012); [b] (Vejsada et al. 2005); [c] (Nakao et al. 2008; Oztop and Shahwan 2006)

310

311

312

This is a preprint, the final version is subject to change, of the American Mineralogist (MSA)
Cite as Authors (Year) Title. American Mineralogist, in press.
DOI: https://doi.org/10.2138/am-2018-6203

313 **FIGURE CAPTIONS**

314 **FIGURE 1.** Cs^+ adsorption on Na-Mica-4, at RT (white circle) and 80º C (black star):
315 a) Adsorption percentage, and, b) K_d.

316 **FIGURE 2.** Adsorption isotherm of Cs^+ on Na-Mica-4 at RT (white circle) and 80 ºC
317 (black star).

318 **FIGURE 3.** SEM microimage and compositional maps of Na-Mica-4 after Cs^+ sorption
319 at a) RT, and, b) 80 ºC.

320 **FIGURE 4.** *001* reflection of Na-Mica-4 before and after Cs^+ adsorption at a) RT, and,
321 b) 80 ºC.

322 **FIGURE 5.** Full XRD patterns of Na-Mica-4 before (marked as M4) and after Cs^+
323 adsorption at 80º C at the indicated initial concentration. Oriented clay mounts in air-
324 dried form (Cu kα radiation).

325 **FIGURE 6.** ^{29}Si MAS NMR spectra of Na-Mica-4 before and after Cs^+ sorption at 80
326 ºC.

327

328

329

330

331

This is a preprint, the final version is subject to change, of the American Mineralogist (MSA)
Cite as Authors (Year) Title. American Mineralogist, in press.
DOI: https://doi.org/10.2138/am-2018-6203

332 ***Figure 1***

333

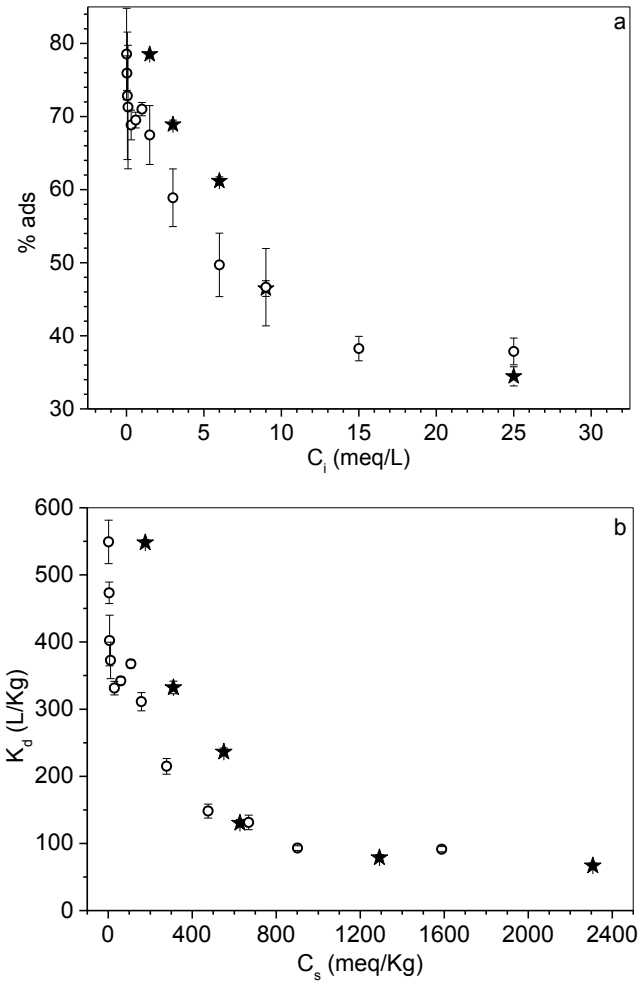

This is a preprint, the final version is subject to change, of the American Mineralogist (MSA)
Cite as Authors (Year) Title. American Mineralogist, in press.
DOI: https://doi.org/10.2138/am-2018-6203

334 ***Figure 2***

335

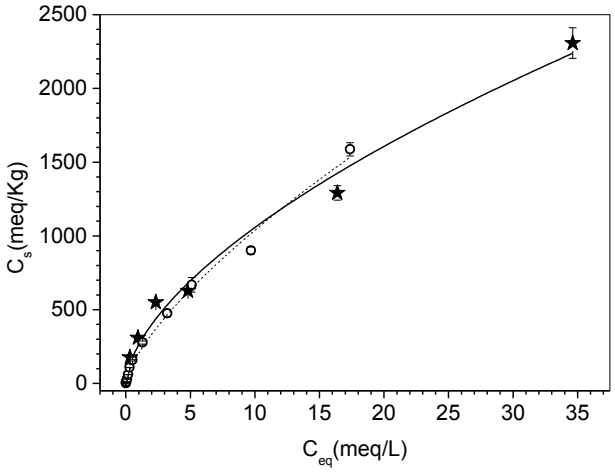

This is a preprint, the final version is subject to change, of the American Mineralogist (MSA)
Cite as Authors (Year) Title. American Mineralogist, in press.
DOI: https://doi.org/10.2138/am-2018-6203

336 ***Figure 3***

337

a

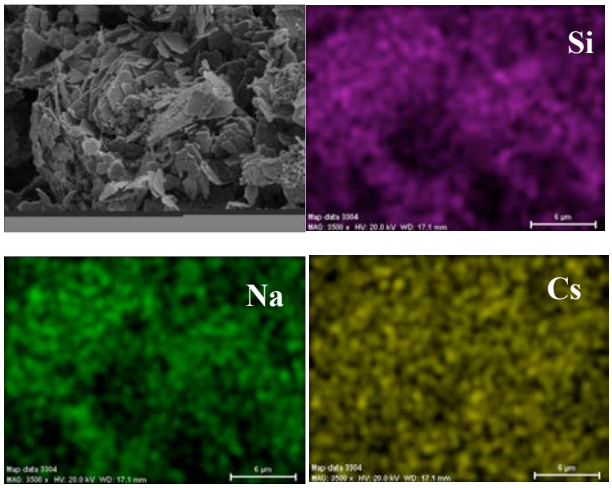

b

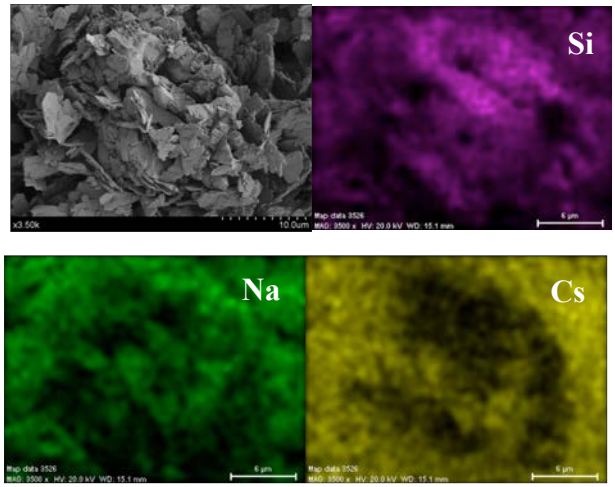

This is a preprint, the final version is subject to change, of the American Mineralogist (MSA)
Cite as Authors (Year) Title. American Mineralogist, in press.
DOI: https://doi.org/10.2138/am-2018-6203

338 ***Figure 4***

339

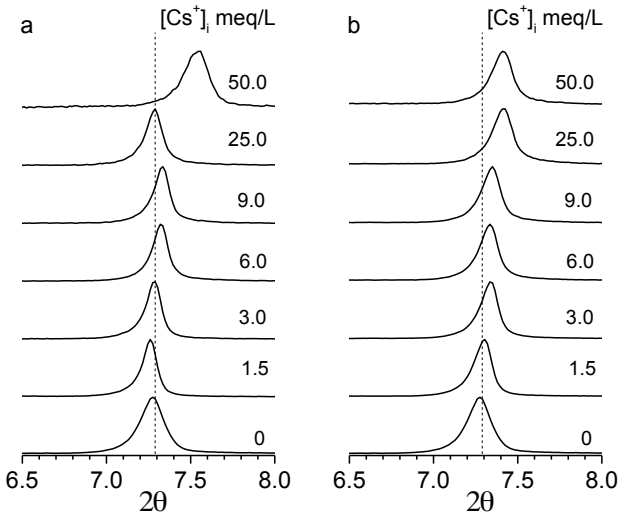

340

341 ***Figure 5***

342

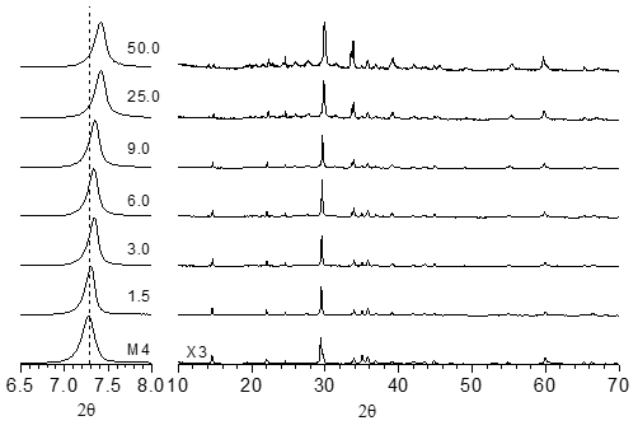

This is a preprint, the final version is subject to change, of the American Mineralogist (MSA)
Cite as Authors (Year) Title. American Mineralogist, in press.
DOI: https://doi.org/10.2138/am-2018-6203

343

344 ***Figure 6***

345

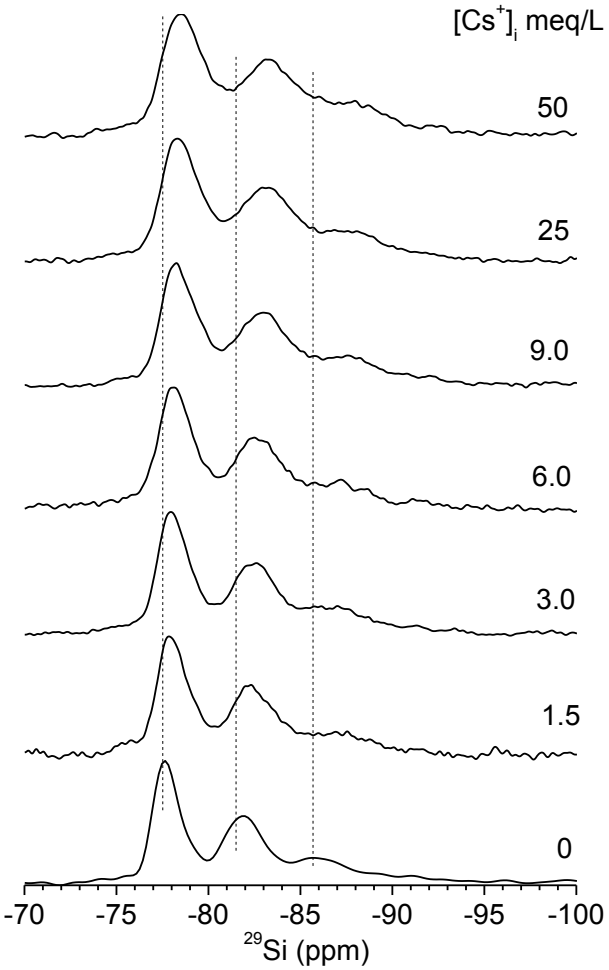

This is a preprint, the final version is subject to change, of the American Mineralogist (MSA)
Cite as Authors (Year) Title. American Mineralogist, in press.
DOI: https://doi.org/10.2138/am-2018-6203

346 **GRAPHICAL ABSTRACT**

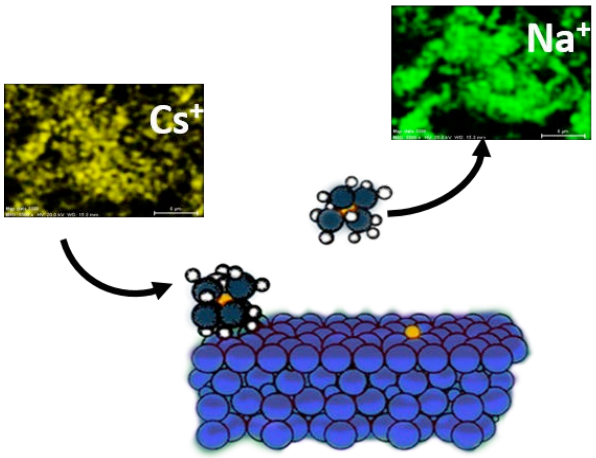

347

348

349